J Mater Sci (2008) 43:5634–5643
DOI 10.1007/s10853-008-2590-5

Effects of strain rate and elevated temperature on electromagnetic radiation emission during plastic deformation and crack propagation in ASTM B 265 grade 2 titanium sheets

V. S. Chauhan · Ashok Misra

Received: 13 October 2007 / Accepted: 11 March 2008 / Published online: 8 July 2008

Abstract Some basic aspects of electromagnetic radiation (EMR) emission during quasi-static plastic deformation and crack propagation in ASTM B 265 grade 2 titanium sheets are reported in this paper. It has been observed that titanium emits several intermittent EMR signals starting near the yield and continuing up to fracture. The EMR emissions are sensitive to the applied strain rates. The number of EMR emissions shows a parabolic variation with strain rate, exhibiting a maxima. It appears that the temporary pinnings of the dislocations injected from the crack tip, which is essential for the emission of EMR as described in a recent model by the authors, do not adequately occur at high as well as low strain rates. At elevated temperatures, the square of the EMR amplitude is observed to be proportional to $\exp(-mU/kT)$, where U is the activation energy for the movement of jogs, k the Boltzmann constant, T the temperature and $m \leq 1.0$.

Introduction

Metal response to deformation depends upon the temperature, level and type of stress applied, strain rate, oxidation and corrosion and other environmental factors. For safe operation of any component under dynamic conditions, understanding the mechanism of plastic deformation and crack initiation is very important. In this context, emission of electromagnetic radiation (EMR) during plastic deformation, crack initiation and crack propagation in metals and alloys, and generation of a high transient magnetic field during crack initiation under tension in ferromagnetic metals and alloys, reported earlier [1–18], appears significant. In a recent paper [18], it has been established that these EMR emissions from metals and alloys are in several ways different from those observed in non-metallic materials such as ionic crystals, rocks, ice, etc.

The EMR emissions from metals and alloys have also been explored and confirmed by Tudik and Valuev [19], Perelman and Khatiashvili [20], Dickinson et al. [21], Jagasivamani [22], Jagasivamani and Iyer [23], Muthukumaran et al. [24] and so on. Molotskii [25] presented a dislocation mechanism for these EMR emissions. Recently, Srilakshmi and Misra [14] reported an additional phenomenon of secondary EMR during plastic deformation and crack propagation in uncoated and metal-coated metals and alloys.

Electromagnetic radiation accompanying the detonation of chemical explosives was reported by Kolsky [26]. Such emissions result from detonations of both bare and cased explosives. However, the dominant wavelengths of emissions from these two types of explosions generally differ by as much as three or four orders of magnitudes. Brown et al. [27] have reported far-field and near-field experimental measurements of electric fields emitted by metal encased explosives and shown that metal fracture is the dominant mechanism leading to these emissions. Further, Brown et al. [28] have also examined the back surface emission of EMR resulting from the impact fracture of mild carbon-steel at strain rates of approximately 10^6/s. They obtained time-domain measurements of two perpendicular components of the electric displacement vector at the distances of up to 20 m from the targets, providing

V. S. Chauhan (✉) · A. Misra
Department of Mechanical Engineering, Birla Institute of Technology, Mesra, Ranchi 835 215, India
e-mail: chauhanvishals@yahoo.com

A. Misra
e-mail: dr_ashok_misra@rediffmail.com

evidence that the EMR emission, previously reported during quasi-static measurements [1–7], is also present during impact fracture of metals.

Titanium and its alloys, due to their exceptional strength-to-weight ratios, low density and high melting points, are the choice-materials for a wide range of applications under hostile environment. Grade 2 titanium is an important material for aircraft and reaction vessel applications. It has good impact properties at low temperatures and excellent resistance to erosion and corrosion. It offers moderate strength and high ductility for fabrication, as evidenced by its typical stress–strain curve.

Since the EMR emission from metals and alloys can well be applied in understanding plastic deformation, in the design of smart sensors/composites [29–31] as well as in evaluation of important mechanical/physical properties [17], it was decided to investigate the effect of strain rate and elevated temperature on EMR emission characteristics in Grade 2 titanium and the results are presented here.

Experimental

The experimental results presented in this paper have been divided into the following three groups: (a) some preliminary experiments, (b) effect of strain rate on EMR emissions and (c) EMR emission characteristics at elevated temperatures. All experiments were conducted under opening mode of fracture.

Material and specimens

Commercially pure titanium, ASTM B265 grade 2 cold-rolled strips of thicknesses 0.7, 1.5, 2.5 and 4.0 mm were investigated. The composition of titanium was: 0.011% C, 0.12% Fe, 0.008% N_2 and rest Ti. All specimens were cut with their longitudinal axes along the rolling direction of the sheets/strips.

For the preliminary investigations, specimens of dimensions 100 mm × 12 mm were cut from 0.7, 1.5, 2.5 and 4.0 mm thick strips. For the EMR emission studies under opening mode of fracture, double initial straight notches, each of length a, were provided at the centre of each specimen, corresponding to initial notch length to specimen width ratio, $2a/w = 0.5$, as per ASTM norms; w is the width of the specimen. This configuration is shown in Fig. 1a.

For the investigation of the effect of strain rate on EMR emission, specimens with dimensions 100 mm × 12 mm were cut from 0.7 mm thick sheet. At the centre of the specimen, a circular notch of 0.5 mm radius was given on both sides, causing a total reduction of 1 mm in its width (Fig. 1b) so as to provide a wider zone for the visual inspection of crack propagation.

For the investigation on EMR emission characteristics at elevated temperature, specimens of dimensions 200 mm × 12 mm × 0.7 mm were prepared as shown in Fig. 1c. A suitably greater length of the specimen had been selected for accommodating the heating element. Initial double edge straight notches of 3 mm each, $2a/w = 0.5$, were provided in these specimens also.

Instrumentation

For preliminary investigation and for the effect of strain rate on EMR emission, the antenna was made of two copper chips of dimensions 10 mm × 10 mm × 0.32 mm pasted on insulation paper. These copper chips were fixed on both sides of each specimen. The insulation paper eliminated the direct contact between the antenna and the specimen surface. The two copper chips were joined electrically (Fig. 1).

The antenna for the investigations on EMR emission at elevated temperatures was made with a 40 mm × 10 mm × 0.32 mm copper chip. It was bent to form a T-shape, open at the bottom. A thin mica sheet was fixed on each specimen for thermal and electrical insulation. The T-shaped antenna was now mounted on the specimen covered by the mica insulation. The configuration is shown in Fig. 1c. This antenna was tested at high temperature environment (up to 550 °C) and was found to be uninfluenced by the thermal noise.

In the tests for preliminary studies and for investigating the effect of elevated temperature, one lead of a 1 MΩ impedance cable was connected to the antenna and the other was connected to a manually operated 1 ton capacity portable Hounsfield tensometer on to which the specimens were mounted for loading. The tensometer was made electrically grounded. In the tests for the investigation of the effect of strain rate on EMR emissions specimens were mounted on Tinius Olsen H100KT universal testing machine (UTM) with Test Navigator software, which had a facility to apply load at constant strain rate. For these tests, one lead of 1 MΩ impedance cable was connected to the antenna and the other was connected to Tinius Olsen H100KT machine, which was made electrically grounded.

For the entire tests mentioned above the electrical cable of the antenna was connected to a 150 MHz analog–digital HAMEG oscilloscope model HM 1507-3 with a built-in software SP107FFT (Beta-version) for recording the signals. An RS 232 interface was used for transferring the data from the oscilloscope to an IBM Pentium IV computer.

The power supply circuit to the band heater is shown in Fig. 1d. In order to suppress the noise produced by the band heater, a cylindrical shield of copper sheet was provided inside the band heater. The variation in the temperature of the specimen was obtained by regulating the

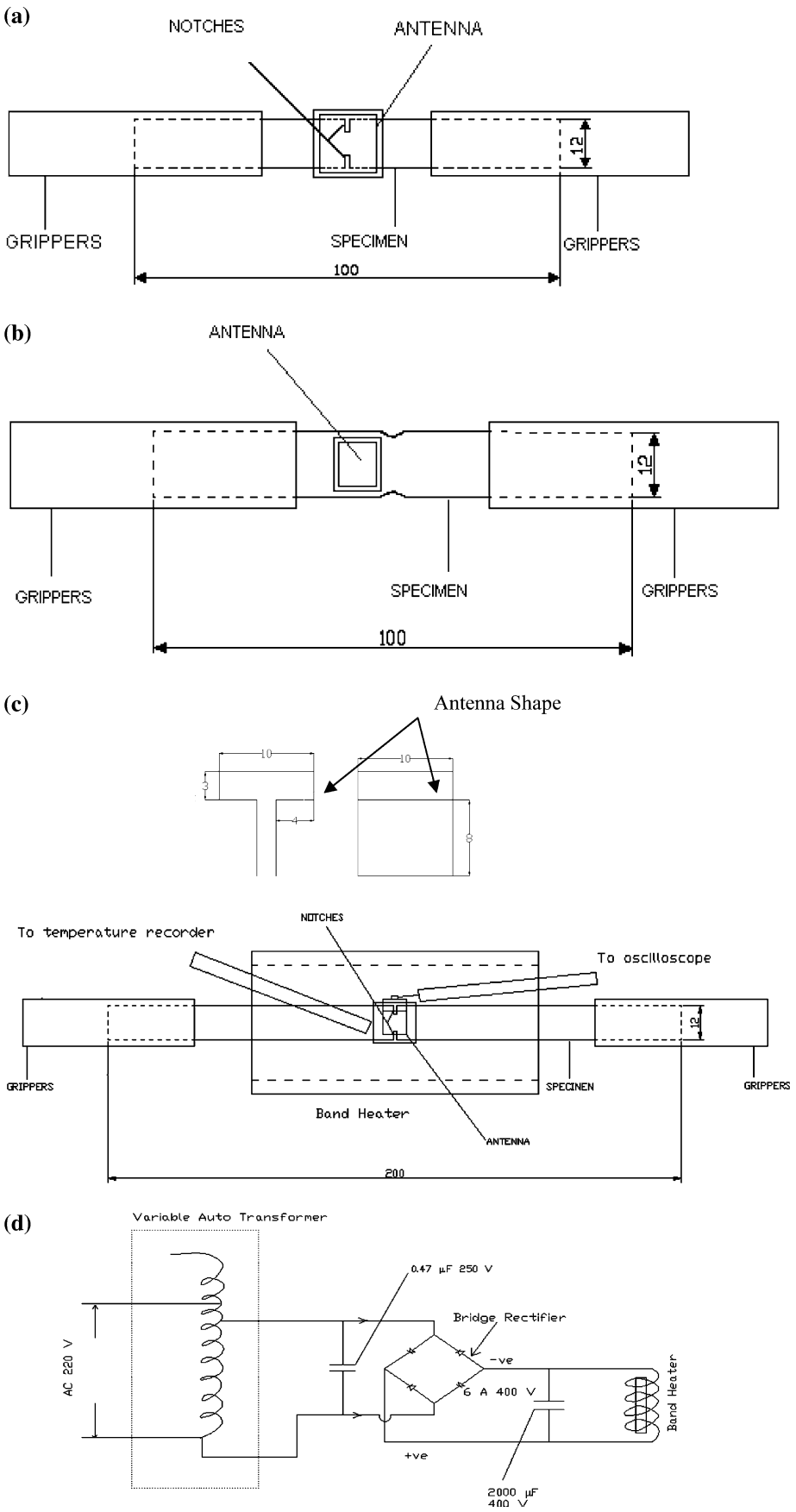

Fig. 1 (**a**) Specimen arrangement for preliminary experiments on EMR emission. (**b**) Loading arrangement for effect of strain rate tests. (**c**) Experimental set up for the elevated temperature experiment. Antenna used is depicted above the figure. (**d**) Power supply circuit for the Band heater

power supply to the heater by the variable voltage autotransformer. A digital temperature indicator (Temperature Measurement Trainer Model-UITM 03) of measuring capacity 0–550 °C was used to measure the instantaneous temperature of the specimen. The antenna and heating arrangement are shown in Fig. 1c.

Results and discussions

Some preliminary experiments

Several EMR emissions were observed during plastic deformation, crack propagation and fracture of ASTM B265 grade 2 titanium sheet specimens of all thicknesses. Figure 2 is a sample print out of the engineering stress versus engineering strain curve of a 0.7 mm thick specimen stressed at a constant engineering strain rate of 41.7×10^{-4}/s (crosshead speed = 15 mm/min). The oscilloscope had to be tuned to "single shot mode" to pick up the transient EMR signals. Once the oscilloscope picked up an EMR signal, it switched off. The UTM crosshead was stopped. It recorded a small stress relaxation in the curve. The picked up EMR signal was transferred to the computer for further processing. The crack tip was visually inspected for any crack initiation and propagation. The oscilloscope was again switched on and further loading on the specimen continued. This process was repeated after each EMR emission. As is evident from Fig. 2, a total of nine EMR signals were emitted from this particular specimen during the entire stressing up to fracture. Point A shows the onset of plastic deformation and point B the start of crack propagation. Thus it is clear from Fig. 2 that the specimen starts emitting EMR signals first near the onset of plastic deformation and then goes on emitting EMR signals intermittently up to fracture. Point 9 is the final fracture.

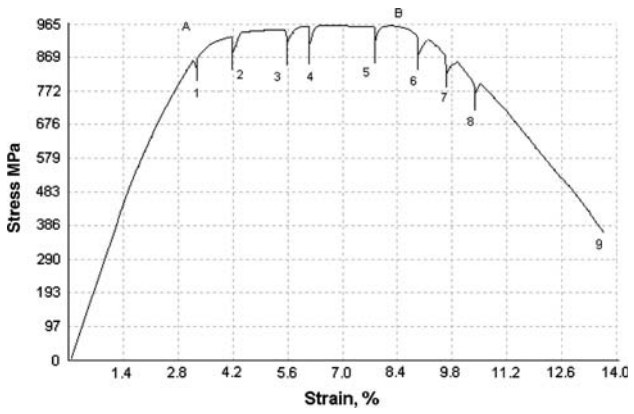

Fig. 2 Engineering stress versus engineering strain curve for an ASTM B265 grade 2 titanium sheet specimen tested at engineering strain rate 41.7 E−4 s^{-1} (crosshead speed 15 mm/min)

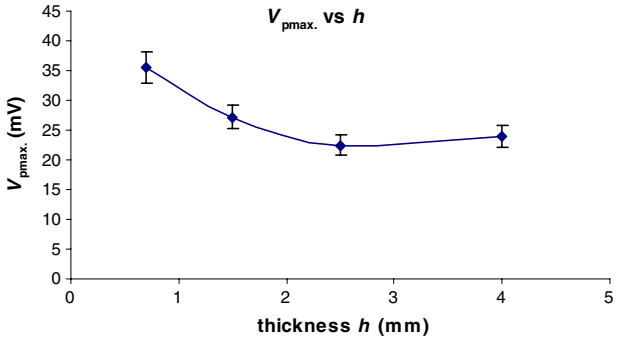

Fig. 3 Variation in maximum amplitude of EMR emission V_{pmax} with thickness h, of the specimens

Figure 3 shows the variation of the magnitudes of EMR amplitudes $|V_{p\max}|$, with the thickness h, of the specimens. All values refer to the last EMR signals emitted prior to final fracture. As mentioned in "Material and specimens" section, for the present experiments, the grade 2 titanium sheets were available in four thicknesses only, viz. 0.7, 1.5, 2.5 and 4.0 mm. It can be seen that the EMR amplitudes show a maxima at 0.7-mm thickness and then gradually attain a nearly constant value for higher thicknesses. Since larger EMR amplitude signals were better for analysis, hence 0.7 mm thick specimens were selected for the investigations on the effects of strain rates and elevated temperatures on EMR emissions.

Further, the experimental data showed a scatter-band of ±5.0–8.0% from the mean value as is expected in experiments on fracture. The scatter-band in the measurements of EMR amplitude, $|V_{p\max}|$ (mV), is shown in Fig. 3 and the subsequent relevant figures.

Since Fig. 3 shows that the EMR amplitude almost becomes constant for higher thicknesses of grade 2 titanium, following the procedure adopted by Kumar and Misra [17] for Cu–Zn alloys, experiments were repeated and the average values of electromagnetic energy release rate A and the elastic strain energy release rate G_{I} under mode I fracture were plotted against thickness for grade 2 titanium. The results are shown in Figs. 4 and 5. Since G_{I} and A were to be studied, the last EMR signals prior to fracture were analysed for Figs. 4 and 5. Here $A = \int V_p^2 \, \mathrm{d}t \Big/ \Delta t$, where the EMR signal V_p versus time t, was converted into V_p^2 versus time curve by the in-built software of the oscilloscope, and Δt is the time duration of $V_{p\max}$ [17]. These figures show a very close similarity between G_{I} and A in grade 2 titanium as well. Therefore, it appears that the measurements of A for the maximum EMR peak can lead to the measurement of the elastic strain energy release rate G_{I} in a specimen, which can further be correlated to the fracture toughness, G_{IC}.

Further, nature of the curve in Fig. 5 suggests a parabolic variation of A/G_{I} with h^{-1} of the type $G_{\mathrm{I}} = CAh^2$,

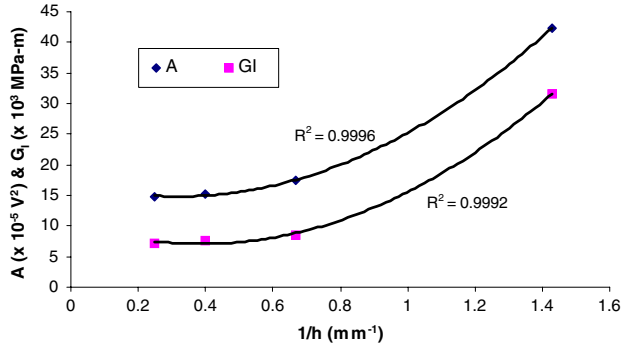

Fig. 4 Variation of elastic strain energy release rate G_I (J/m^2) and electromagnetic energy release rate A (μV^2) with 1/h in ASTM B265 grade 2 titanium sheets

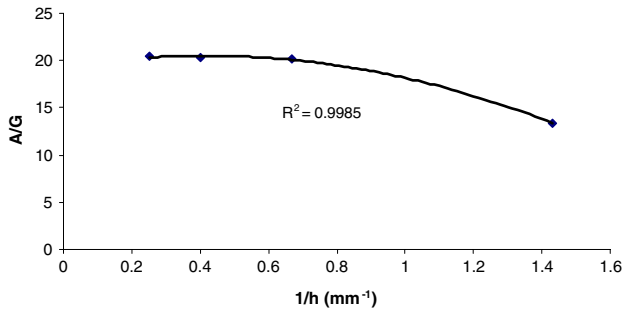

Fig. 5 Variation of A/G_I with 1/h

for thinner sheet specimens. C is the constant of proportionality. which depends on the material properties.

Effect of strain rate on EMR emissions

Experiments were then conducted on 0.7-mm thick grade 2 titanium sheet specimens at constant crosshead speeds of 0.5, 1.0, 5.0, 10.0, 15.0 and 20 mm/min.

The true strain rate $\dot{\varepsilon}$, corresponding to each constant crosshead speed v_{CH}, was calculated according to the formula [32],

$$\dot{\varepsilon} = \frac{(v_{CH}K/AE) + \dot{\varepsilon}_p}{(KL/AE) + 1}, \tag{1}$$

where v_{CH} is the constant speed of the crosshead of the machine, K the machine stiffness, A the instantaneous area of the cross-section of the specimen, L the instantaneous gauge length of the specimen, E the Young's modulus of elasticity of the specimen material, and $\dot{\varepsilon}_p$ the true plastic strain rate.

It may be noted here that both $\dot{\varepsilon}$ and $\dot{\varepsilon}_p$ depend upon the instantaneous strain. Therefore, ε_p was calculated at the instant of each EMR emission prior to crack propagation (point B in Fig. 2) by calculating ε and ε_E by the formulae [32],

$$\varepsilon = \ln(e+1), \quad \varepsilon_E = \ln(e_E+1), \tag{2}$$

where e is the conventional strain, the subscript E refers to the elastic limit, and

$$\varepsilon_p = \varepsilon - \varepsilon_E. \tag{3}$$

Figure 6 shows a sample plot of average value of ε_p versus time at the crosshead speed $v_{CH} = 15$ mm/min, for the specimen of Fig. 2. An average value of $\dot{\varepsilon}_p$ was evaluated from Fig. 6, and substituted in Eq. 1 to give $\dot{\varepsilon}$. By this method, the average true strain rates were calculated corresponding to $v_{CH} = 0.5$, 1.0, 5.0, 10.0, 15.0 and 20.0 mm/min as 1.264×10^{-4}, 2.572×10^{-4}, 11.957×10^{-4}, 23.988×10^{-4}, 38.42×10^{-4} and 50.452×10^{-4} s^{-1}, respectively. For the Tinius Olsen testing machine, $K = 0.2$ MN/m; initial gauge length of the specimen $L_0 = 60$ mm and $E = 117$ GPa for ASTM titanium grade 2.

Experiments over the past several years [1–24] have shown that the EMR signals (voltage versus time curve) during plastic deformation and fracture of metals and alloys are of two broad nature: (i) damped oscillatory and (ii) exponentially decaying. During the experiments for the effect of strain rate on EMR emissions, both kinds of signals were observed in grade 2 titanium as well. Figure 7a ($|V_{p\max}| = 13$ mV) and b ($|V_{p\max}| = 4$ mV) shows sample printouts of the signals emitted at average true strain rates of 23.988×10^{-4} and 11.957×10^{-4} s^{-1}, respectively.

Some other features common to all the sets of tests are as follows:

1. Maximum number of signals were emitted before the crack tip propagation.
2. Signals prior to A (Fig. 2) were absent at lowest and highest strain rates tested viz. 1.264×10^{-4} and 50.452×10^{-4} s^{-1}, respectively.
3. Maximum number of signals were emitted at crosshead speed of 5 mm/min corresponding to strain rate $\dot{\varepsilon} = 11.957 \times 10^{-4}$ s^{-1}.
4. Majority of signals were exponential in nature at all strain rates.

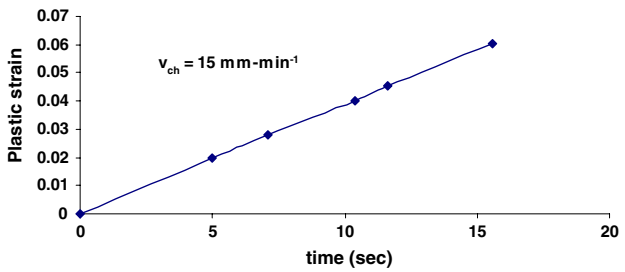

Fig. 6 Plot of true plastic strain with time for a specimen tested at a crosshead speed of 15 mm/min

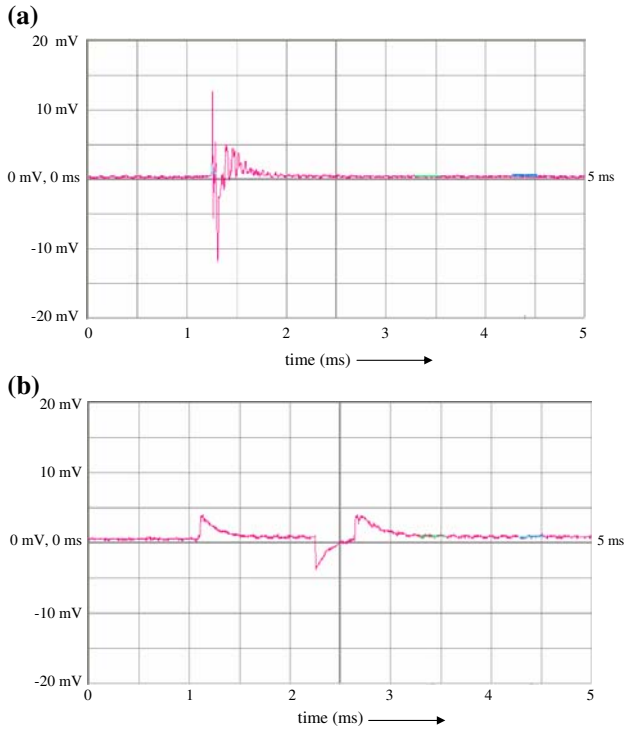

Fig. 7 (**a**) Sample printout of a damped oscillatory signal emitted during tests for the effects of strain rate on EMR emission. (**b**) Sample printout of an exponentially decaying signal emitted during tests for the effects of strain rate on EMR emission

5. Maximum number of damped oscillatory signals were observed at the average true strain rate of $\dot{\varepsilon} = 23.988 \times 10^{-4}\ s^{-1}$ corresponding to the crosshead speed of 10 mm/min.
6. EMR amplitudes of damped oscillatory signals were in general much larger (10–25 mV) than the exponential EMR amplitudes (1–4 mV) at all strain rates.

Figure 8 is a plot of the maximum peak amplitude of EMR emission versus strain rate. It shows a maxima at strain rate of $23.988 \times 10^{-4}\ s^{-1}$. Figure 9 is a plot of total number of signals (average value) emitted by a specimen during stressing against the strain rate. *This excludes the EMR signal at final fracture, which is invariably emitted from all metallic specimens under all circumstances*. Since the effect of strain rate on the correlation of EMR emission with plastic deformation and crack propagation was to be investigated, this prompted the exclusion of the EMR signal at final fracture in the analysis.

Figure 10 is a plot of average number of signals emitted before crack propagation (point B in Fig. 2). A close similarity can be observed in the curves of Figs. 9 and 10. Total number of EMR signals emitted prior to final fracture as well as the number of signals emitted before crack propagation are less at the lower strain rates, attain a maxima at a strain rate of $11.957 \times 10^{-4}\ s^{-1}$, and then

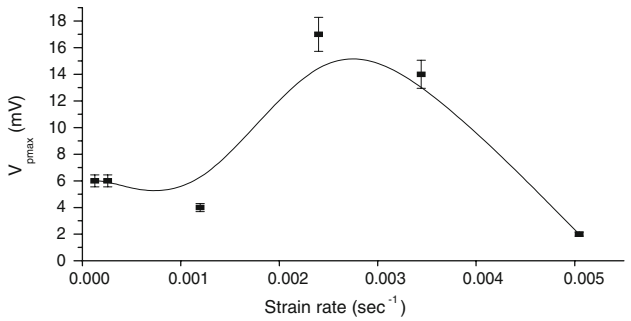

Fig. 8 Plot of maximum amplitude of EMR emission versus strain rate in ASTM B265 grade 2 titanium sheet specimens

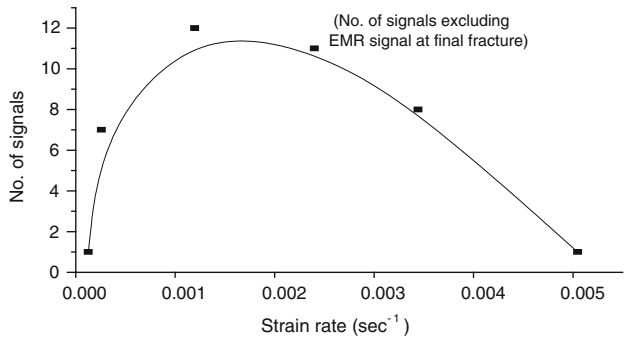

Fig. 9 Plot of total number of EMR signals emitted (excluding EMR signal at final fracture) versus strain rate in ASTM B265 grade 2 titanium sheet specimens

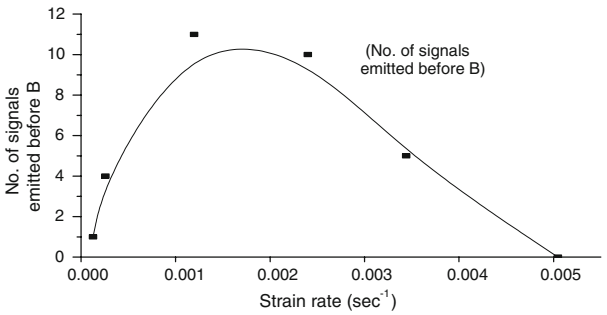

Fig. 10 Plot of number of EMR signals emitted before B versus strain rate in ASTM B265 grade 2 titanium sheet specimens

again become less as the strain rate is increased. From Fig. 10 it is further seen that the strain rates higher than $50.452 \times 10^{-4}\ s^{-1}$, i.e., fast fractures do not promote any EMR emission prior to crack propagation and fracture. This conclusion is also supported from the observations of Brown et al. [27, 28] where they have reported EMR only during fracture from the high strain rate fracture of mild carbon-steel and from the detonation of metal encased explosives, respectively.

Based on Molotskii's model [25], Misra et al. [18] have recently proposed a generalized theoretical model for the EMR emissions from metallic materials. The essential

concept is as follows: with the increase in the externally applied stress beyond the critical resolved shear stress in a sheet specimen, a plastic zone is created ahead of the crack tip. Dislocations from the crack tip spread both above and below the plane of fracture. In order to fracture the specimen by this process, more dislocations have then to be injected into the existing plastic zone. As the crack spreads, each edge dislocation injected from the tip of the crack into the yield line pushes the existing dislocations further along these lines until general yielding is eventually produced [33]. It is well known that an electrostatic potential is built around an edge dislocation in an inhomogeneously strained crystal and the dislocation behaves as an electric line dipole [34]. It is, therefore, imagined that an edge dislocation injected from the crack tip *gets temporarily pinned-up at its two ends*, before spreading along the yield lines. These pinnings could be due to impurity atoms, network points, jogs, etc. As a result, a time-varying bending is induced in the dislocation under the action of the stress. This bending of the dislocation produces a time-varying increase in its length, hence a time-varying increase in the electric line dipole moment and gives rise to the EMR emission.

Therefore, the observed EMR emission in metals is essentially originated due to *the temporary pinning of the two ends of the edge dislocation* before it is pushed along the yield lines by the other newly injected dislocations from the crack tip. This temporary pinning of the dislocation ends will, therefore, depend upon the speed and force of the freshly injected dislocations which push the concerned dislocation along the yield lines, self-energy of the dislocation, and also upon the pinning forces of the impurities, etc.

Therefore, at high strain rates, since the plastic deformation occurs rapidly, freshly injected dislocations with high speed, overcome the pining forces at the two ends of the dislocation ahead of them, which results in a decrease in the number and the amplitude of EMR emissions. This is in conformity with the experimental results (Figs. 8–10).

On the other hand, at low strain rates since the rate of plastic deformation is low, accumulation of the pinnings at the two ends of the dislocation may not be adequate enough to cause any temporary pinning, again resulting in decrease in the number and the amplitude of EMR emissions (Figs. 8–10).

It further appears that in metals the EMR emission occurs by two mechanisms: (i) by the bending of dislocations as described above, and (ii) by the bending of dislocations superimposed by the ionic oscillations due to breakage of atomic bonds which essentially occurs during fracture. The fact that the EMR responses (amplitude and frequency) bear a close relationship with bond energy of metals has earlier been reported [11].

Effect of elevated temperature on EMR emission in titanium

For the elevated temperature tests specimens had to be fractured fast to avoid any temperature drop due to radiation losses during the experiments. This resulted in the recording of only one EMR emission near the initial notch tip instability in each specimen. Further, the antenna used during elevated temperature tests (Fig. 1c) had larger surface area as compared to the antenna for strain rate tests (Fig. 1b), it amplified the amplitudes of EMR signals to 50–250 mV range.

Figure 11 is the plot of average tensile stress values S_t at which the EMR signals were obtained versus temperature for the ASTM grade 2 titanium sheet specimens. Figure 12 shows the variation of EMR amplitude with temperature.

In order to understand the EMR effects at elevated temperature, imagine a moving dislocation AB coming across a row of intersecting ones whose mean spacing is l, as shown in Fig. 13. To cut through the row, a segment l of AB has to move a distance of order b, where b is the Burgers vector. During the process of cutting, each segment of AB bows out as shown in Fig. 13. It is well known that the intersections of dislocations create jogs. The energy of formation of a jog U_j is of the order of $U_j = \alpha G b^3$, where G is the shear modulus and $\alpha \cong 0.2$ for most metals. If τ be the external shear stress acting on the dislocation AB, the work done on AB in moving it a distance b, is $\tau l b^2$. When $\tau l b^2$ is greater than U_j the dislocation AB can cut through without help from thermal fluctuations, but otherwise an activation energy

$$U = U_j - \tau l b^2 = \alpha G b^3 - \tau l b^2 \tag{4}$$

is needed [35]. It may be noted here that G and τ are temperature dependent. The yield stress is practically given by the condition $U = 0$ or $\tau = \tau_y = \alpha G b / l$. Under ambient conditions, for $\tau > \tau_y$, $\tau l b^2$ is generally greater than $\alpha G b^3$

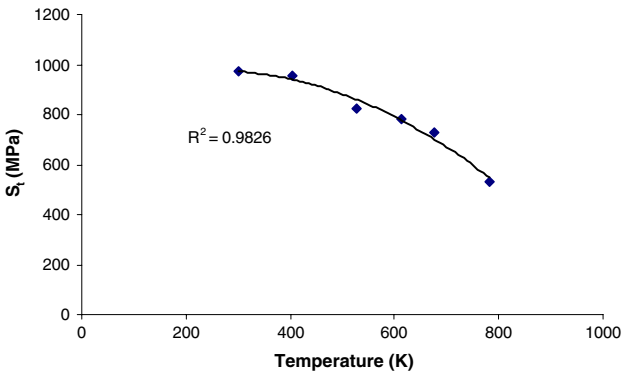

Fig. 11 Variation in maximum tensile stress at crack tip instability S_t with temperature in 0.7 mm ASTM B265 grade 2 titanium sheet specimens

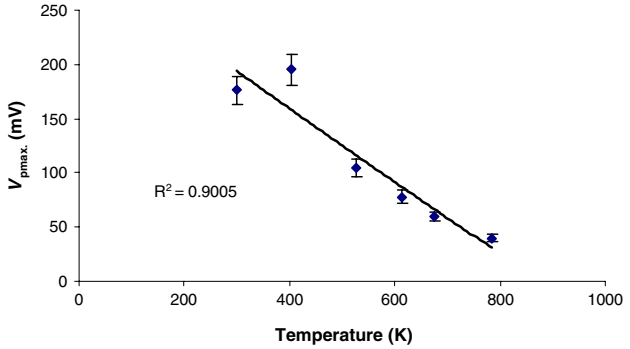

Fig. 12 Variation in maximum amplitude of EMR emission with temperature in 0.7 mm ASTM B265 grade 2 titanium sheet specimens

in metals. Hence the dislocation AB cuts through the rows of intersecting dislocations. During this process the segments of AB bow out, and the increment in the segment length increases the electric line dipole moment giving rise to the EMR emission [18, 25].

However, when the metal specimen under an applied shear stress τ is heated to an elevated temperature T, stress recovery occurs. Therefore, in order to continue the cutting process by the dislocation AB, some additional energy must be supplied by the thermal fluctuations. Let this additional energy be mU, where $m \leq 1.0$.

Now assuming a Boltzmann distribution for the frequency of cutting through the rows of intersecting dislocations, the number n of the segments of dislocations like AB is written as

$$n = n_0 \exp\left[-\frac{mU}{kT}\right] = n_0 \exp\left[-\frac{m(\alpha Gb^2 - \tau lb^2)}{kT}\right], \quad (5)$$

where k is the Boltzmann constant, and n_0 is the thermodynamic equilibrium number of spacings between the intersecting dislocations defined by the condition $U = 0$ or $\tau = \alpha Gb/l$.

Now during the bowing out, each dislocation segment at temperature T will emit EMR as described above. The total EMR amplitude $V_{\max}$ is then proportional to $\sqrt{n}$ under random phase approximation [18]. Hence

$$V^2_{\max.} = A_0 \exp\left[-\frac{mU}{kT}\right] = A_0 \exp\left[-\frac{m(\alpha Gb^3 - \tau lb^2)}{kT}\right], \quad (6)$$

where A_0 is the constant of proportionality times n_0. Equation 6 may be rewritten as

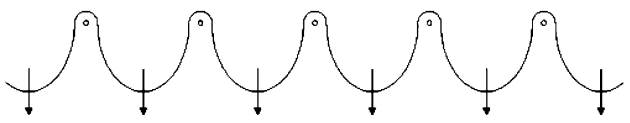

Fig. 13 A dislocation line held up by a row of intersecting dislocations [36]

$$\log\left(V^2_{\max}\right) = \log A_0 - \frac{mU}{kT} = \log A_0 - \frac{m(\alpha Gb^3 - \tau lb^2)}{kT} \quad (7)$$

Therefore, a plot of $\log\left(V^2_{\max}\right)$ versus mU/kT should be linear in nature at elevated temperature. Incidentally, $V^2_{\max}$ is also proportional to the intensity of radiation. Hence, the intensity of radiation appears to vary linearly with U/kT which is reasonable to expect.

As regards the experimental verification of Eq. 7, variation of Young modulus E with temperature for ASTM grade 2 titanium sheet was obtained from standard reference [36] and the corresponding G values were calculated at the desired temperatures. Assuming the yield stress in tension as 0.8 times the tensile strength S_t, of titanium [36], the shear stress values τ were evaluated approximately as $\tau = (0.577)\ (0.8\ S_t)$, from Fig. 11, where 0.577 is the von-Mises yield criterion factor.

The spacing between the intersecting dislocations l is not exactly known at different temperatures. However, the yield stress is practically equal to $\alpha Gb/l$ [35]. Hence ignoring the temperature effects, an average value of l is estimated as $l \sim \alpha Gb/\tau_y$ at ambient conditions. This gives $l \sim 100b$, estimating a density ρ of intersecting dislocations ($\rho \sim l^{-2}$) of 10^{15} m^{-2}, which is a reasonable value [35].

With the above values of the parameters in Eq. 7, a linear variation of $\log\left(V^2_{\max}\right)$ versus U/kT with a correlation coefficient $R^2 = 0.9904$ was obtained as shown in Fig. 14, exhibiting an experimental verification of Eq. 7. In Fig. 14, $V_{\max}$ is the average of $|V_{p\max}|$ values at each temperature. When this graph is extrapolated to ambient temperature using the data of Figs. 11 and 12 [at $T = 300$ K, $\log\left(V^2_{\max}\right) = 10.342$ and $U/kT = -187.974$], a slight drop in the straight line of Fig. 14 is observed at $T = 300$ K. This shows that when thermal fluctuations start dominating *then only* the square of EMR amplitude is proportional to $\exp(-U/kT)$ as suggested in Eq. 6. Further, from Fig. 14, $m \sim 0.02$, for titanium.

One point is noteworthy here. An increase in EMR amplitude with increase in temperature was reported in

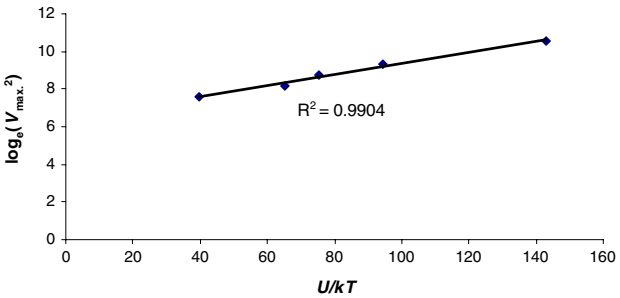

Fig. 14 Plot of $\log\left(V^2_{\max}\right)$ versus mU/kT in ASTM B265 grade 2 titanium sheet specimens

copper contrary to a decrease in EMR amplitude observed in plain-carbon steel [11] and aluminium [13]. While reporting the EMR characteristics at elevated temperatures in aluminium [13] it was concluded that the observed increase in EMR amplitude with increase in temperature in copper results from the recombination of partial dislocations at elevated temperatures in metals with low stacking fault energy only. Figure 12 further confirms this conclusion in titanium which has a high stacking fault energy of 0.15 J/m^2 as compared to copper (0.04 J/m^2). Therefore, for metals with low stacking fault energy, Eq. 6 will require some modifications, and will be worth investigating.

Further, in an earlier work [13] the electromagnetic energy release was assumed to be proportional to hf, where h is Planck constant, and thermal energy imparted to the dislocations proportional to kT, and a smooth variation was obtained when V_{pmax} was plotted against hf/kT for aluminium (f.c.c.). Now in the case of titanium (h.c.p.) also, a parabolic variation exhibiting a maxima has been obtained as shown in Fig. 15. However, the nature of variation is different in the two cases; titanium shows a maxima at $hf/kT \sim 2.75 \times 10^{-9}$, while aluminium exhibited a minima at $hf/kT \sim 3.7 \times 10^{-8}$.

Finally, Fig. 16, the plot of average minimum dominant EMR frequency versus temperature, validates the prediction

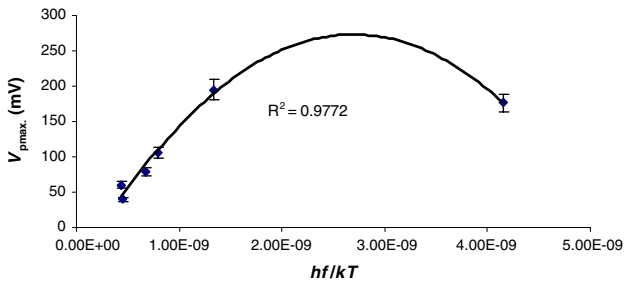

Fig. 15 Variation of maximum amplitude of EMR emission $V_{p\max}$ versus hf/kT in ASTM B265 grade 2 titanium sheet specimens

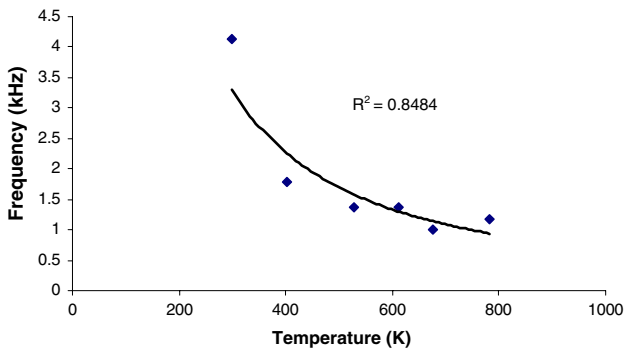

Fig. 16 Variation in minimum dominant EMR frequency with temperature in 0.7 mm ASTM B265 grade 2 titanium sheet specimens

from Molotskii Model [25] in h.c.p. metal, titanium as well. Thus Molotskii's prediction that EMR frequency should decrease with increase in temperature has been verified in b.c.c. [11], f.c.c. [13] and h.c.p. metals.

Conclusions

On the basis of the results and discussions presented above, following conclusions are drawn:

(i) EMR emission is sensitive to strain rate; number of EMR emissions during plastic deformation is very less at small as well as high strain rates; it shows a maxima at a strain rate of 11.957×10^{-4} s^{-1} in ASTM grade 2 titanium.

(ii) At high strain rates, freshly injected dislocations with high speed, overcome the pinning forces at the two ends of the dislocation ahead of them which results in a decrease in the number and amplitude of EMR emissions.

(iii) On the other hand, at low strain rates, accumulation of pinnings at the two ends of the dislocation is not adequate enough to cause any temporary pinning, which again results in a decrease in the EMR emission.

(iv) At elevated temperatures intersection of dislocations creating jogs favour the EMR emission. The square of EMR amplitude is observed to be proportional to $\exp(-mU/kT)$, where U is the activation energy for the movement of jogs, and $m \leq 1.0$.

(v) ASTM grade 2 titanium also endorses the conclusion that an increase in EMR amplitude at elevated temperature results from the recombination of partial dislocations at elevated temperatures in metals with low stacking fault energy only.

Acknowledgement Research grant from the Department of Science and Technology, Government of India, is gratefully acknowledged.

References

1. Misra A (1973) Indian J Pure Appl Phys 11:419
2. Misra A (1975) Nature (Lond) 254:133. doi:10.1038/254133a0
3. Misra A (1975) cited in Ninth yearbook to the encyclopedia of science and technology. Edizioni Scientific E Techniche, Mondadori, Italy
4. Misra A (1977) Phys Lett 62A:234
5. Misra A (1978) Appl Phys 16:195. doi:10.1007/BF00930387
6. Misra A (1981) J Sci Ind Res 40:22
7. Misra A, Ghosh S (1980) Indian J Pure Appl Phys 18:851
8. Mishra D, Misra A (1980) Neurol India XXVIII:234
9. Misra A, Ghosh S (1981) Appl Phys 23:387. doi:10.1007/BF00903221
10. Misra A, Varshney BG (1990) J Magn Magn Mater 89:159. doi:10.1016/0304-8853(90)90720-B

11. Misra A, Kumar A (2004) Int J Fract 127:387. doi:10.1023/B:FRAC.0000037676.32062.cb
12. Kumar A, Misra A (2005) J Magn Magn Mater 285:71. doi:10.1016/j.jmmm.2004.07.017
13. Srilakshmi B, Misra A (2005) Mater Sci Eng A 404:99. doi:10.1016/j.msea.2005.05.100
14. Srilakshmi B, Misra A (2005) J Mater Sci 40:6079. doi:10.1007/s10853-005-1293-4
15. Srilakshmi B, Misra A (2005) Manuf Tech Res Int J 1:97
16. Kumar R, Misra A (2006) J Zhejiang Univ Sci A 7(11):1800
17. Kumar R, Misra A (2007) Mater Sci Eng A 454–455:203. doi:10.1016/j.msea.2006.11.011
18. Misra A, Prasad RC, Chauhan VS, Srilakshmi B (2007) Int J Fract 145:99. doi:10.1007/s10704-007-9107-0
19. Tudik AA, Valuev NP (1980) Sov Tech Phys Lett 6:37
20. Perelman ME, Khatiashvili NG (1980) Bull Acad Sci Georgian SSR 99:357
21. Dickinson JT, Jenson LC, Bhattacharya SK (1985) J Vac Sci Technol 3:1398. doi:10.1116/1.572788
22. Jagasivamani V (1987) Some studies on the electromagnetic and acoustic emissions associated with deformation and fracture of metallic materials. PhD Dissertation, I.I.T., Madras
23. Jagasivamani V, Iyer KJ (1988) Mater Lett 6:418. doi:10.1016/0167-577X(88)90043-2
24. Muthukumaran S, Kumar P, Pandey VK, Mukherjee SK (2008) Int J Adv Manuf Technol 36:249. doi:10.1007/s00170-006-0840-8
25. Molotskii MI (1980) Sov Tech Phys Lett 6:22
26. Kolsky H (1954) Nature 173:77. doi:10.1038/173077a0
27. Brown W, Schmidt M, Dzwilewski P, Samaras T (2005) Electromagnetic emissions in case of detonation of metal encased explosives. Proceedings of 14th APS Topical Conference on Shock compression of Condensed Matter, Baltimore, MD, July 31–August 5
28. Brown W, Schmidt M, Calahan K (2005) Electromagnetic radiation from the high strain rate fracture of mild carbon-steel. Proceedings of 14th APS Topical Conference on Shock compression of Condensed Matter, Baltimore, MD, July 31–August 5
29. Srilakshmi B, Misra A (2004) Electromagnetic radiation during crack propagation in metals—a new trend in the development of smart materials. Proceedings of International Symposium on Smart Materials and Systems, Chennai, India, 15–17 December
30. Srilakshmi B, Misra A (2005) Development of smart materials through electromagnetic radiation in metal coating. Proceedings of International Symposium on Intelligence based Materials and Manufacturing, Ranchi, India, 18–20 August
31. Kumar R, Misra A (2006) A new approach for smart sensors in design against metallic failure. International Conference on Resource Utilization and Intelligent System, Erode, India, 4–6 January
32. Dieter GE (1988) Mechanical metallurgy. Mc Graw-Hill Book Co., London, p 295
33. Cottrell AH (1963) Proc R Soc A 276:1
34. Nabarro FRN (1967) Theory of crystal dislocations. Clarendon Press, Oxford, p 615
35. Cottrell AH (1953) Dislocations and plastic flow in crystals. Clarendon Press, Oxford, p 174
36. Boyer R, Welsch G, Collings EW (1994) Materials properties handbooks: titanium alloys. ASM International, p 178